The Anisotropy of Surface-Emitted Infrared Radiation Characterized With Satellite Data

W. L. Smith, Jr., M. M. Khaiyer
AS&M, Inc.
Hampton, Virginia USA

P. Minnis and D. F. Young
Atmospheric Sciences Division
NASA Langley Research Center
Hampton, Virginia, USA

L. E. Egli
Swiss Federal Institute of Technology (ETH)
Zurich, Switzerland

Proceedings of ALPS 99 Symposium
Meribel, France
18-22 January 1999
WK2-P-17, pp. 1,4

THE ANISOTROPY OF SURFACE-EMITTED INFRARED RADIATION CHARACTERIZED WITH SATELLITE DATA

Smith Jr., William L. , Khaiyer, Mandana M. and Doelling, David R.
Analytical Services & Materials, Inc., Hampton, VA 23666 USA

Minnis, Patrick
Atmospheric Sciences Division, NASA Langley Research Center, Hampton, VA 23681 USA

Egli, Luca
Swiss Federal Institute of Technology (ETH), Zurich, Switzerland

Introduction

Surface-emitted infrared radiation has typically been assumed to be invariant with respect to angular conditions, except for viewing-zenith-angle (VZA) dependent limb darkening and surface emissivity. However, recent studies reveal significant anisotropy in the outgoing infrared radiance field due to angular variations, as uneven terrain and vegetation cover lead to differential solar radiative heating. Wong et al. (1996) analyzed helicopter data as well as Geostationary Operational Environmental Satellite (GOES) data to examine the magnitude of infrared anisotropy on a large scale for several surface types. They found brightness temperature differences (BTD's) up to 5 K for simultaneous measurements from two GOES satellites with different viewing geometries. Lagourde and Kerr (1993) measured infrared brightness temperature variations of up to 8 K with a detector 2 m above the surface at various VZA's across various surface types. Canopy temperature variations dependent on both VZA and relative azimuth angle (RAZ) have been measured on a small scale (McGuire et al., 1988). Several modeling studies have demonstrated that an azimuthal variation in temperature should occur due to canopy structure (McGuire et al., 1988) and extreme terrain morphology (Lipton et al., 1997). The dependence of brightness temperature on RAZ, VZA, solar zenith angle (SZA), topography and vegetation cover, however, observations or models, although some theoretical models have been developed to account for some of these dependencies (e.g. Sobrino and Casselles, 1990). In this paper, BTD's estimated from multiple satellites (GOES-8, GOES-9 and GOES-10) viewing the same scenes are examined and classified according to viewing and solar zenith angles, as well as the time of day, International Geosphere Biosphere Programme (IGBP) scene type, and surface roughness. From these comparisons, the validity of applying the isotropy assumption to longwave radiation emitted by different scene types is evaluated. The results have important implications for the determination of clear-sky longwave fluxes derived from satellite data for cloud and radiation budget studies such as the new Clouds and Earth's Radiant Energy System (CERES) and the upcoming European Geostationary Earth Radiation Budget (GERB) instrument. The anisotropy is especially critical for the fixed viewing angles of GERB. These anisotropic effects also influence estimation of surface skin temperature from operational meteorological satellites. Preliminary results indicate that shortwave bidirectional reflectance models may be used as part of a method to correct for the longwave anisotropy.

Data and Methodology

GOES-8, 9, and 10 4-km-resolution imager datasets from various cloud-free days

satellites were spaced at 75°W, 135°W and ~105°W, respectively. The infrared (IR, 10.8 μm) data from each satellite were sectioned into 2^o x 2^o regions at various locations across North America. Within each region, the data were further subdivided into 10' sub-boxes to assign an International Geosphere Biosphere Programme (IGBP; Belward and Loveland, 1996) vegetation type. The IGBP scene types were grouped into 3 broader vegetation categories, namely, forest, open shrub and flatland. The flatland category includes the grass and cropland IGBP types. A more concise breakdown of this categorization will be given at the conference. The average IR radiance was calculated and converted to a mean temperature T at a given time for each 10' sub-box. The sub-box temperatures were then averaged for the 3 broad vegetation categories within each region. The effect of the intervening atmosphere on the observed temperatures was removed with a radiative transfer model that accounts for the absorption and emission in each atmospheric layer. Optical depths for each layer are based on the temperature and humidity profile from the closest 3-hourly, 60-km resolution Rapid Update Cycle analyses (Benjamin et al., 1994) or the nearest radiosonde measurements. The correlated-*k* distribution approach (Kratz, 1995) was used to determine each layer optical depth. This correction yields the apparent surface skin temperature $T_s(Gx)$, where Gx is the satellite indicator and x is the satellite number. This quantity is designated "apparent" because it has not been corrected for surface emissivity. The radiative transfer model of Fu and Liou (1993) was used to compute OLR(Gx) based on the observed values of T_s and the temperature and humidity profiles.

The brightness temperature difference,

$$\mathrm{BTD_x} = T_s(G8) - T_s(Gx),$$

between two of the GOES satellites constitutes a measure of anisotropy. It is assumed that BTD = 0 represents a reflectance distribution functions (BRDF) for the GOES visible channel were taken from the model of Minnis and Harrison (1984) as a measure of the solar reflectance anisotropy. These models are designated by the variable $\chi(\theta_o,\theta,\phi)$, where θ_o, θ, and ϕ are the solar zenith, viewing zenith and relative azimuth angles, respectively. The topography for each region is characterized by its mean altitude Z and the standard deviation of altitude σ_z within the region. Values for these parameters were derived from the 10' elevation maps of the U.S. Navy (available from U.S. Geological Survey).

Results

Figure 1 depicts apparent surface temperatures derived from GOES-8, 9 and 10 on 3 April 1998 for a relatively flat region (σ_z is 125 m) in northwest Texas (region A at 32.5N and 102.5W) consisting primarily of grassland. The diurnal cycles all differ even though two of the satellites (GOES-8 and 9) view the region from nearly the same θ. Examination of the diurnal cycles for other

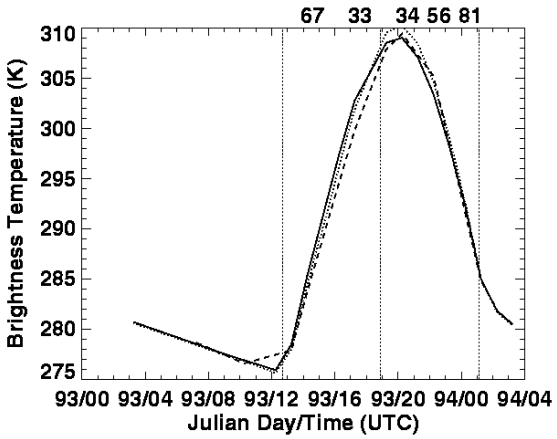

Fig 1. Brightness temperature curves (10.8 um) on 3 and 4 , 1998 for region A. Solid, dashed and dotted lines denote GOES-8, 9 and 10 brightness temperatures, respectively. Solar zenith angles are labelled on the top axis. The vertical lines represent sunrise, local noon, and sunset.

not shown here indicates phase or time differences of up to 1 hour in peak T_S for the different satellites. In general, T_S for the satellite east of a region's longitude is warmer

afternoon relative to the more westerly satellite. Figure 2 shows the time series of both BTD_9 and BTD_{10}. The latter ranges from about 1K to –1K , while the former reaches almost 3K in the morning before dropping to –2K in the afternoon.

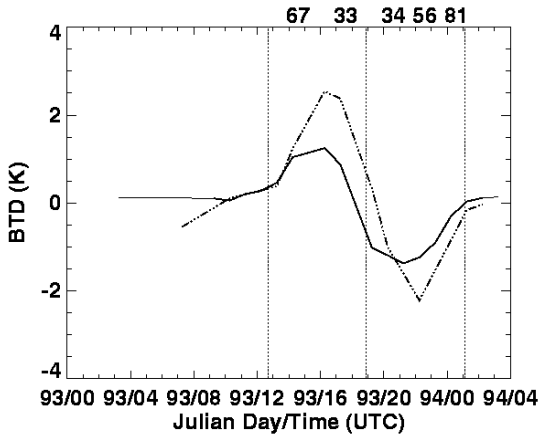

Fig 2. Brightness temperature difference (BTD) curves for the same region and time period as in Fig. 1, for GOES-8 minus GOES-10 (solid) and GOES-8 minus GOES-9 (dot-dashed).

Results from a region B located in south-central New Mexico (33.0N 105.0W) on the same day are shown in Figure 3. Region B consists of forested mountains, rolling shrub and grasslands (σ_z is 413 m). Here, the BTD

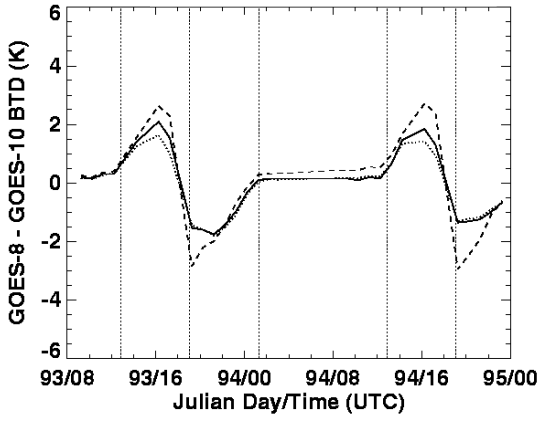

Fig 3. GOES-8 minus GOES-10 BTD for three generalized scene types in region B : grassy land (solid line), forested land (dashed), and shrub land (dotted).

curves are plotted for each of the three general scene types. BTD_{10} for flatland reaches a value of 2 K, slightly larger than that of region A; however, the BTD_{10} of forested land reaches about 2.5K, over twice the value of BTD_{10} for region A. The minimum values of noon instead of late afternoon as seen for region A. The relative differences between regions B and A are similar for BTD_9 (not shown). The maxima for BTD_9, found between 900 and 1000 LT, reach almost 5K for the forested boxes. The minima, ~ -3K, are lower than those in region A and occur earlier in the afternoon. Both BTD_9 and BTD_{10} repeat the same patterns the following day.

To ensure that these differences are not due to some spurious diurnal cycles in the GOES IR channels, BTD_9 and BTD_{10} were computed for open water in the Sea of Cortez. In both cases, the BTDs vary by less 0.3K over the course of the day. Over nearby coastland, the ranges in BTD_9 and BTD_{10} are 7 and 4K, respectively. Thus, it is clear that the observed brightness temperatures differ primarily because of differences in the temperatures of the respective land structures observed by a given satellite.

To illustrate the potential impact of these BTD variations on clear-sky longwave flux, the OLR was computed from the time series of T_s for each satellite over various regions. The results for region B (Fig. 4) yield OLR differences from 7 to -7 (4 to -3) Wm^{-2}

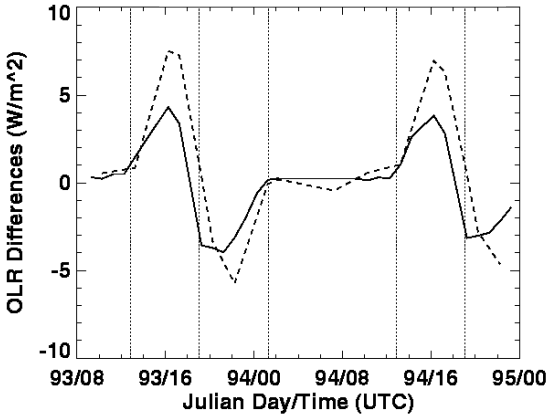

Fig 4. OLR differences for IGBP scene type 10 (grassland) computed for same region and period as in Fig. 3, for GOES-8 minus GOES-9 (dashed) and GOES-8 minus GOES-10 (solid).

for G8-G9 (G8-G10). A more mountainous region in central Mexico (σ_z of 916 m), region C (25.0N 107.0W), was found to yield even

The mean daytime OLR (G8-G9) differences and their standard deviations for region B (C) are 1.5 ± 4.6 Wm^{-2} (2.5 ± 9.7 Wm^{-2}). Over the flatter terrain of region A, the daytime OLR differences have a mean and standard deviation of 1.5 ± 3.6 W/m^2. At night, OLR differences are slight except during early evening.

Discussion

Given the results presented here, it is clear that the OLR derived from geostationary satellites will be biased at a given local time and, perhaps, on average if the anisotropy is ignored. Similarly, satellites in mid-inclined orbits such as the Earth Radiation Budget Satellite or the TRMM satellite will have biases that are unlikely to average out over a month. Coincident data from airborne instruments and the Visible Infrared Radiometric Scanner aboard the TRMM satellite will be used to estimate these biases at some of the relative azimuth and viewing zenith angles not observed with GOES (to be presented at the conference). From a remote sensing perspective, a simple approach to account for IR anisotropy is desirable. The anisotropy of reflected solar radiation over land provides a relative measure of illumination for a particular set of angles. For example, the maximum reflectance generally occurs at the antisolar point, while the minimum reflectance occurs at the angles for which shadowing is greatest. In Fig. 5, a comparison is shown between BTD's and differences in the bidirectional reflectance factors(χ,) for GOES-8 and 10 for regions A, B and C. The correlations are excellent ($r^2 \sim$ 0.93, 0.98 and 0.97, respectively). and the slope increases with increasing σ_z. Similar results have been found for other regions not discussed here. These initial correlations suggest that the BDRF factors and σ_z could serve as the primary parameters in a model of the BTD angular dependence.

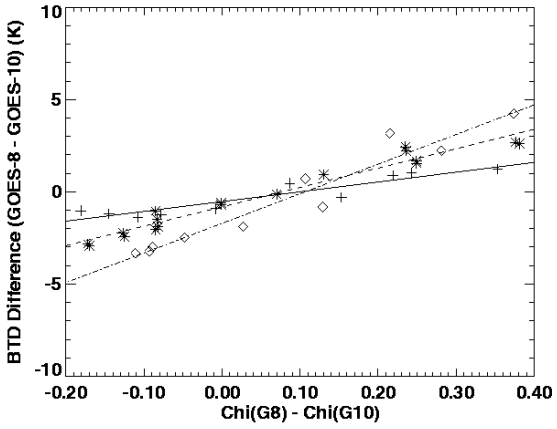

Fig 5. Differences (GOES-8 minus GOES-10) in Bidirectional Reflectance Distribution Factors (BRDF) plotted against the corresponding BTD's for region A grassland (plus signs, solid line), forested regions B (asterisks, dotted line) and C (diamonds, dot-dashed line)

References

Benjamin, S.G., J.M. Brown, K.J. Brundage, B.E. Schwartz, T. G. Smirnova, and T. L. Smith, 1998: The operational RUC-2. *Proc. AMS 16th Conf. Weather Anal. and Forecasting*, Phoenix, AZ, 249-252.

Belward, A. and T. Loveland, 1996: The DIS 1km land cover data set. In *Global Change*, The IGBP Newsletter, #27, Sep., 1996.

Fu, Q. and K.-N. Liou, 1992: On the correlated k-distribution method for radiative transfer in nonhomogeneous atmospheres. *J. Atmos. Sci.*, **49**, 2139-2156.

Kratz, D. P., 1995: The correlated *k*-distribution technique as applied to the AVHRR channels. *J. Quant. Spectrosc. Rad. Transf.*, **53**, 501-507.

Lagourde, J.P. and Y. Kerr, 1993: Experimental study of angular effects on brightness surface temperature for various types of surfaces. *Proc. of the Workshop on Thermal Remote Sensing of the Energy and Water Balance over Vegetation in Conjunction with Other Sensors*. Sept. 20-23, 1993, La Londe Les Maures, France, 107-111.

Lipton, A. E. and J. M. Ward, 1997: Satellite-view biases in retrieved surface temperatures in mountain areas. *Remote Sens. Environ.*, **60**, 92-100.

McGuire, M. J., L. K. Balick, J. A. Smith, and R. A. Hutchison, 1988: Modeling directional thermal radiance from a forest canopy. *Remote Sens. Environ.*, **27**, 169-186.

Minnis, P. and E. F. Harrison, 1984: Diurnal variability of regional cloud and clear-sky radiative parameters derived from GOES data. Part III: November 1978 radiative parameters. *J. Climate Appl. Meteorol.*, **23**, 1032-1052.

Sobrino, J. A. and V. Caselles, 1990: Thermal infrared radiance model for interpreting the directional radiometric temperature of a vegetative surface. *Remote Sens. Environment*, **33**, 193-199.

Wong, T., P. Minnis, and C.H. Whitlock, 1996: Anisotropy of surface-emitted radiation. *IRS '96: Current Problems in Atmospheric Radiation*, Aug. 19-24, 1996, Fairbanks, Alaska, 457-460.